the thermal decomposition of $(C_8H_{14})B(pz)\cdot Hpz$ (=$H^+[(C_8H_{14})B(pz)_2]^-$) is possible but is not very suitable for the preparation of the pyrazabole $(C_8H_{14})B(\mu\text{-}pz)_2B(C_8H_{14})$, since the adduct sublimes even under atmospheric pressure.

The FD mass spectrum of $(C_8H_{14})B(\mu\text{-}pz)_2B(C_8H_{14})$ exhibited not only the molecular ion cluster at $m/z$ 376 but also one at $m/z$ 188. This observation suggests that the $B_2N_4$ ring of the pyrazabole readily undergoes symmetrical cleavage to yield the monomer. This same feature was previously been observed for some *B*-amino-substituted pyrazaboles,[11] and trigonal 1-pyrazolylboranes have been found to exist under normal conditions only when the boron is also bonded to two additional nitrogen atoms and is incorporated into a cyclic structure. This latter feature is likely to be a consequence of electronic saturation of the boron atom, although the boron atom of trigonal 1-pyrazolylboranes shows Lewis acidity.[12-14] On the other hand, the suggested ease of the symmetrical cleavage of the pyrazabole $(C_8H_{14})B(\mu\text{-}pz)_2B(C_8H_{14})$ and the unusual NMR observations on $(C_8H_{14})B(pz)\cdot Hpz$ (see above) may well be due to steric rather than electronic factors.

The reaction of $(C_8H_{14})B(pz)\cdot CH_3NH_2$ with 9-BBN proceeded according to eq 2. The resulting $(C_8H_{14})B(\mu\text{-}pz)(\mu\text{-}NHCH_3)B(C_8H_{14})$ (**1**, X = $NCH_3$) is a relative of the pyrazabole $(C_8H_{14})B(\mu\text{-}pz)_2B(C_8H_{14})$, where one of the two bridging pz groups is replaced by a bridging $NHCH_3$ moiety. Analogous pyrazabole relatives have previously been obtained from the reaction of borazines, $(RBNR')_3$, with Hpz,[3] and similar species (**1**, X = O, S, Se) were recently prepared from the reaction of $(C_8H_{14})BXB(C_8H_{14})$ with Hpz.[2]

$$(C_8H_{14})B(pz)\cdot CH_3NH_2 + \tfrac{1}{2}[(C_8H_{14})BH]_2 \xrightarrow{-H_2} (C_8H_{14})B(\mu\text{-}pz)(\mu\text{-}NHCH_3)B(C_8H_{14}) \quad (2)$$

**Acknowledgment.** This was work was supported by the Office of Naval Research, and travel funds by the Alexander von Humboldt Foundation are also gratefully acknowledged (K.N.).

(11) Niedenzu, K.; Seelig, S. S.; Weber, W. *Z. Anorg. Allg. Chem.* **1981**, *438*, 51-62.
(12) Weber, W.; Niedenzu, K. *J. Organomet. Chem.* **1981**, *205*, 147-156.
(13) Alam, F.; Niedenzu, K. *J. Organomet. Chem.* **1982**, *240*, 107-119.
(14) Alam, F.; Niedenzu, K. *J. Organomet. Chem.* **1983**, *243*, 19-30.

Contribution from the Department of Chemistry, University of South Carolina, Columbia, South Carolina 29208

# $^{113}$Cd Shielding Tensors of Cadmium Compounds. 5. Single-Crystal Studies of the Dimer of Diaquobis(2-hydroxybenzoato)cadmium(II) and Tetrakis(4-picoline)(nitrato-*O*,*O*')(nitrato-*O*)cadmium(II)

Michael A. Kennedy and Paul D. Ellis*

*Received June 28, 1989*

The orientation of the $^{113}$Cd chemical shielding tensors in single crystals of the dimer of diaquobis(2-hydroxybenzoato)cadmium(II), i.e. Cd-salicylate, and tetrakis(4-picoline)(nitrato-*O*,*O*')(nitrato-*O*)cadmium(II), i.e. Cd-picoline, has been determined. The isotropic chemical shift was determined to be -31 ppm for Cd-salicylate and +11 ppm for Cd-picoline. The space group symmetry of the Cd-salicylate crystal generates two magnetically distinct cadmium lattice sites. The assignment of each experimentally determined tensor to its respective lattice site was not possible due to the special geometry of the ligands in the lattice, which is discussed in the text. However, the two possible orientations differ only slightly and it is therefore possible to interpret the orientation with respect to the ligand identity and geometry. In either case, the most deshielded element is oriented nearly perpendicular to a plane containing two water oxygen atoms. The most shielded element is oriented nearly perpendicular to a pentagonal best least-squares (BLS) plane defined by two pairs of bidentate benzoate oxygen atoms and one monodentate benzoate oxygen atom. The crystal of Cd-picoline generates two crystallographically distinct cadmium sites in the lattice. Two methods were used independently to assign the two experimentally determined tensors to each lattice site. The first method utilizes the empirical observations of shielding contributions of nitrogen versus oxygen ligand donors. The second method exploits the angular dependence of the line width as a function of rotation angle due to dipolar coupling between the spin $I = {}^1/_2$ $^{113}$Cd nucleus and the spin $I = 1$ $^{14}$N nuclei. The two methods consistently assign each tensor to a respective lattice site. At each lattice site, the most deshielded tensor element is oriented nearly orthogonal to a BLS plane of nitrogen atoms defined by four monodentate picoline ligands. Also, at each lattice site, the most shielded element is nearly perpendicular to a plane defined by the $Cd^{2+}$ ion and the two bidentate nitrate oxygen atoms.

## Introduction

Since 1983, single-crystal NMR experiments of cadmium coordination complexes have been carried out to establish the factors that determine both the magnitude and orientation of the chemical shielding tensor elements of the $^{113}$Cd nucleus.[1] In parts 1[1a] and 2[1b] of this series, Honkonen et al. and Honkonen and Ellis examined all oxygen coordination complexes in order to interpret $^{113}$Cd shielding tensor data contemporarily being gathered on all oxygen-metal-coordinated $Ca^{2+}$- and $Zn^{2+}$-containing proteins in the solid phase, e.g. Conconavalin A,[2] parvalbumin,[3] troponin C,[4] calmodulin,[5] and insulin.[6] In these proteins, the $Cd^{2+}$ ion was substituted for the native ion because of its favorable NMR properties, e.g. spin $I = {}^1/_2$ and favorably high relative receptivity, 155 and 11 compared to $^{43}$Ca ($I = {}^7/_2$) and $^{67}$Zn ($I = {}^5/_2$), respectively. The use of model compounds for proteins is necessary for several reasons, e.g. inability to grow adequate protein crystals, mainly because of size or stability constraints and because of the

(1) (a) Honkonen, R. S.; Doty, F. D.; Ellis, P. D. *J. Am. Chem. Soc.* **1983**, *105*, 4163. (b) Honkonen, R. S.; Ellis, P. D. *J. Am. Chem. Soc.* **1984**, *106*, 5488.
(2) Palmer, A. R.; Bailey, D. B.; Cardin, A. D.; Yang, P. P.; Behnke, W. D.; Ellis, P. D. *J. Am. Chem. Soc.* **1978**, *100*, 5236.
(3) (a) Darkenberg, T.; Lindman, B.; Cavê, A.; Parello, J. J. *FEBS Lett.* **1978**, *92*, 346. (b) Cavê, A.; Parello, J.; Drakenberg, T.; Thulin, E.; Lindman, B. *FEBS Lett.* **1979**, *100*, 148.
(4) Forsen, S.; Thulin, E.; Lilja, H. *FEBS Lett.* **1979**, *104*, 123.
(5) Forsen, S.; Thulin, E.; Darkenberg, T.; Krebs, J.; Seamon, K. *FEBS Lett.* **1980**, *117*, 189.
(6) Sudmeier, J. L.; Bell, S. J.; Strom, M. S.; Dunn, M. F. *FEBS Lett.* **1981**, *212*, 560.

0020-1669/90/1329-0541$02.50/0 

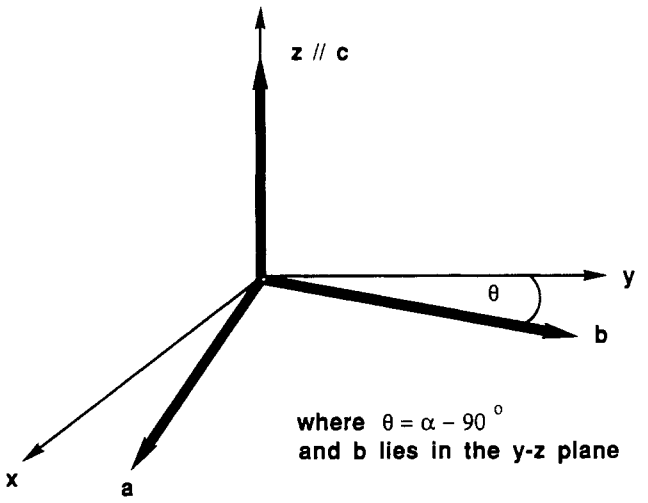


**Figure 1.** Schematic diagram of the geometry defined by Rollett[14] for the derivation of the matrix that projects an oblique unit cell basis $(a,b,c)$ onto an orthogonal axis frame $(x,y,z)$.

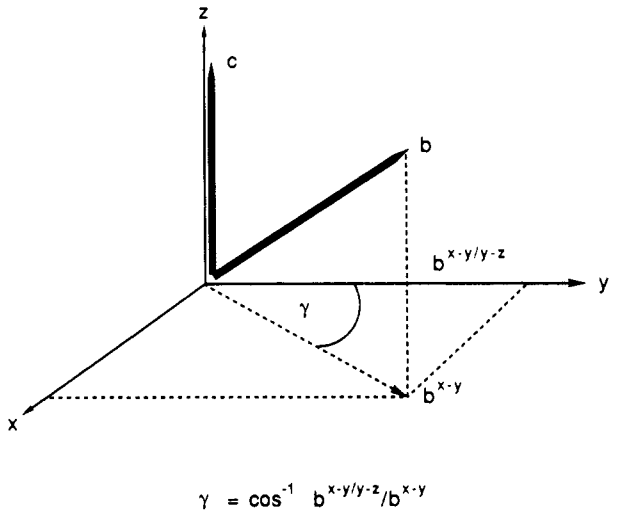


$$\gamma = \cos^{-1} b^{x-y/y-z}/b^{x-y}$$

**Figure 2.** Schematic diagram of the relative geometry between the orthogonal axis frame $(x,y,z)$ and the natural unit cell axes $(a,b,c)$ when the $c$ axis is aligned with the $z$ axis. The projected vectors ($b^{x-y} = b(x',y',0)$ and $b^{x-y/y-z} = b(0,y',0)$) necessary to determine the third non-true Euler angle, $\gamma$, are illustrated.

low percentage by weight of cadmium in protein samples, consequently requiring prohibitively long data collection times. Regardless of the constraint of using model compounds, important knowledge has been gained in understanding shielding contributions of various ligand types and ligand geometries. Specifically, it has been determined that ligated water oxygen atoms are the most deshielding oxygen ligands.[1] Furthermore, the most shielding contributions are determined by the longest Cd–ligand bonds.[1,7] It has been established that the deshielding contribution of a ligand correlates to the degree of covalent character of the Cd–ligand bond;[8] i.e., in general, for monodentate ligands, oxygen contributes greater shielding than nitrogen, which in turn contributes more shielding than sulfur.[9] However, Marchetti et al.[8] have demonstrated that if, by geometrical constraint, a Cd–N bond is longer than a Cd–O bond in the same coordination sphere, the longer bond interaction provides greater shielding to the cadmium nucleus.[8] Effectively, the geometrical constraint can cancel the normal shielding contribution of the nitrogen ligand, which is correlated with a reduction in the covalent character of the bond. Obviously, more progress must be achieved to empirically disentangle all the factors that contribute to the shielding of the cadmium nucleus in coordination compounds and proteins. Therefore, we continue to investigate, by NMR spectroscopy, single crystals of inorganic cadmium complexes, namely, Cd–salicylate and Cd–picoline.

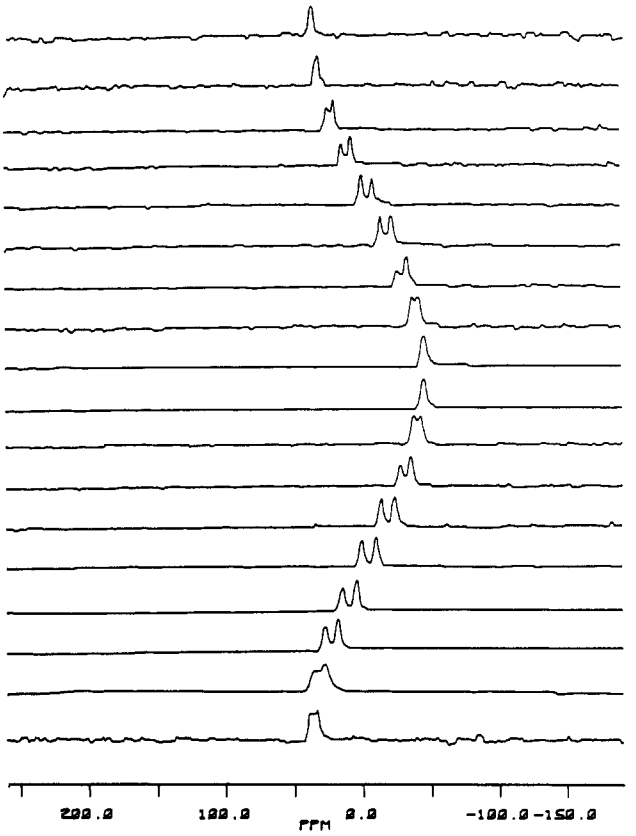


**Figure 3.** Rotation plot for Cd–salicylate about the $a^*$ axis of the orthogonalized unit cell. The bottom spectrum is at 0° rotation angle, whereas the top spectrum is at 180° rotation angle. Intervening spectra were obtained at 10° intervals. Data acquisition parameters are described in the text.

**Table I.** Direction Cosines Relating the Principal Elments of the $^{113}$Cd Shielding Tensor to the Molecular Reference Frame in Cadmium Hydroxybenzoate Dihydrate[a]

| tensor element[b] | chem shift, ppm[c] | direction cosines | | | angles, deg | | |
|---|---|---|---|---|---|---|---|
| | | $a'$ | $b$ | $c'$ | $a'$ | $b$ | $c'$ |
| | | A. Site No. 1 | | | | | |
| $\sigma_{11}$ | −84 | 0.9836 | 0.1482 | 0.1024 | 10 | 81 | 84 |
| $\sigma_{22}$ | −44 | 0.0940 | 0.0631 | −0.9935 | 85 | 86 | 173 |
| $\sigma_{33}$ | 41 | −0.1537 | 0.9869 | 0.0481 | 99 | 9 | 87 |
| $\bar{\sigma}$ | −29 | | | | | | |
| | | B. Site No. 2 | | | | | |
| $\sigma_{11}$ | −86 | −0.9765 | 0.1328 | −0.1696 | 167 | 82 | 99 |
| $\sigma_{22}$ | −46 | 0.1700 | −0.0076 | −0.9854 | 80 | 90 | 170 |
| $\sigma_{33}$ | 39 | 0.1322 | 0.9911 | 0.0151 | 82 | 8 | 89 |
| $\bar{\sigma}$ | −31 | | | | | | |

[a] Eigenvectors and corresponding angles are with respect to the orthogonalized unit cell, $a'$, $b$, $c'$. Site no. 1 and site no. 2 refer to the two unassigned experimentally determined shielding tensors. [b] The convention used for labeling the shielding tensor elements is according to that of Haeberlen, which ascribes $\sigma_{33} = \sigma_{zz}$ = the unique tensor element: Haeberlen, U. *High Resolution NMR in Solids*; Advances in Magnetic Resonance, supplement; Academic Press: New York, 1976. [c] The $^{113}$Cd chemical shifts are reported with positive values to higher frequency/lower shielding relative to solid $Cd(ClO_4)_2 \cdot 6H_2O$.

(7) Kennedy, M. A.; Ellis, P. D.; Jakobsen, H. J. *Inorg. Chem.*, following paper in this issue.
(8) Marchetti, P. S.; Bank, S.; Bell, T. W.; Kennedy, M. A.; Ellis, P. D. *J. Am. Chem. Soc.* **1989**, *111*, 2063.
(9) Ellis, P. D. *Science* **1983**, *221*, 1141.

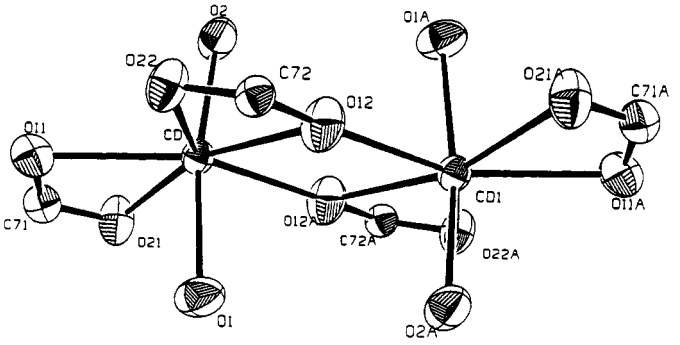


**Figure 4.** Ortep diagram, demonstrating the dimer structure of Cd–salicylate at the *xyz* lattice site. The center of the dimer defines a crystallographic center of symmetry. The letter A following an atom number indicates an atom position generated by an inversion symmetry operation on the corresponding undesignated atom; e.g., O(11A) is generated by operating on the coordinates of the O(11) atom with an inversion operation.

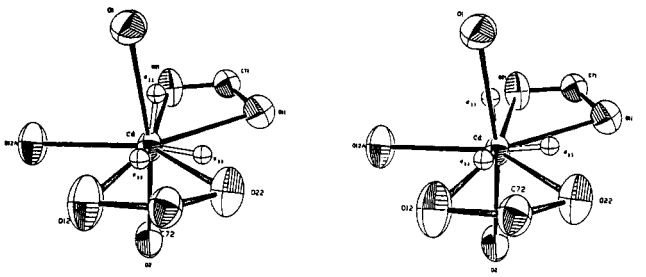


**Figure 5.** Ortep diagrams, showing the immediate coordination sphere of the unique atoms in the complex of Cd–salicylate with (a) site A tensor and (b) site B tensor displayed in the molecular reference frame.

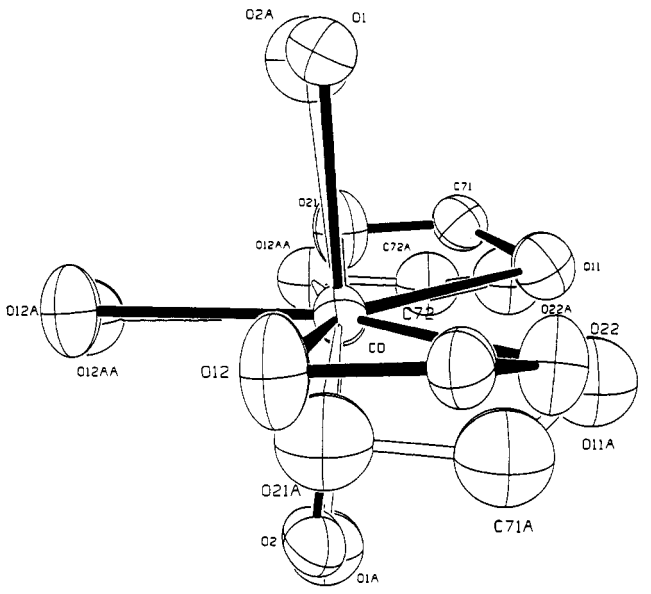


**Figure 6.** Ortep diagram, showing the different orientation of the Cd–ligand geometry for Cd–salicylate at the *xyz* lattice site (light bonds) and 2-fold-related site (dark bonds) translated to a common origin with respect to the natural unit cell basis.

## Experimental Section

Bis($\mu$-*o*-hydroxybenzoato)bis(*o*-hydroxybenzoato)tetraaquodicadmium(II) crystals were grown as described by Charles et al.[10] The crystals are monoclinic ($a$ = 7.747 Å, $b$ = 12.455 Å, $c$ = 15.725 Å, $\beta$ = 96.23°, $Z$ = 4) and belong to the $P2_1/a$ space group.

Tetrakis(4-picoline)(nitrato-*O*,*O*′)(nitrato-*O*)cadmium(II) crystals were prepared as described by Li et al.[11] and doped with 0.1% $Cu(NO_3)_2$ to reduce the $^1$H $T_1$, which facilitated shorter data aquisition times. The copper-doped crystals were confirmed to be isomorphous with the undoped crystals via crystallography. The crystals are triclinic ($a$ = 15.94 Å, $b$ = 18.03 Å, $c$ = 9.84 Å, $\alpha$ = 96.36°, $\beta$ = 102.42°, $\gamma$ = 84.33°) and belong to the $P\bar{1}$ space group.

NMR data were collected, for Cd–salicylate, on a wide-bore Bruker WP-200 spectrometer[12] using a Doty probe (Doty Scientific Inc.). NMR data were collected, for Cd–picoline, on a narrow-bore Varian XL-300 spectrometer using a Doty probe (Doty Scientific Inc.). Data aquisition was via a standard Hartman–Hahn spin-locked cross-polarization pulse sequence.[13] An aquisition time of 51.2 ms preceded by a 2.0-ms contact was used in each case. A relaxation delay of 2 s was typical. Extraction of the chemical shielding tensor from the $^{113}$Cd shift data has already been described.[1]

**Crystallographic Orientation of Oblique Crystals with Respect to an Orthogonal Cube Frame.** Orientation of a unit cell with respect to a cube frame has been described for orthorhombic and monoclinic cases.[1a] The chemical shielding tensor is orthogonal by nature. In order to represent the orientation of the shielding tensor in the molecular frame, any nonorthogonal unit cell basis must be orthogonalized prior to projection of the tensor elements onto the atom of interest. Accordingly, the crystallography must relate the basis of the orthogonalized unit cell to the orthogonal cube reference frame. We use the algorithm of Rollett[14] for orthogonalization of monoclinic and triclinic crystal classes. The natural $c$ axis is aligned with the $z$ axis of the orthogonal frame, and the $b$ axis is rotated into the $y$–$z$ plane of the orthogonal frame (see Figure 1).

**Table II.** Structural Data for Cadmium Hydroxybenzoate Dihydrate: Interatomic Distances and Angles for the Primary Coordination Sphere and Details of Tensor Ligand Geometry in Site No. 1

| | | | |
|---|---|---|---|
| Interatomic Distances, Å | | | |
| Cd–O(1) | 2.300 | Cd–O(12) | 2.535 |
| Cd–O(2) | 2.243 | Cd–O(12′) | 2.271 |
| Cd–O(11) | 2.429 | Cd–O(22) | 2.314 |
| Cd–O(21) | 2.322 | | |
| Interatomic Angles, deg | | | |
| O(1)–Cd–O(2) | 170 | O(11)–Cd–O(21) | 54 |
| O(1)–Cd–O(11) | 92 | O(11)–Cd–O(12) | 134 |
| O(1)–Cd–O(21) | 85 | O(11)–Cd–O(12A) | 149 |
| O(1)–Cd–O(12) | 80 | O(11)–Cd–O(22) | 82 |
| O(1)–Cd–O(12A) | 84 | O(21)–Cd–O(12) | 163 |
| O(1)–Cd–O(22) | 88 | O(21)–Cd–O(12A) | 94 |
| O(2)–Cd–O(11) | 96 | O(21)–Cd–O(22) | 136 |
| O(2)–Cd–O(21) | 94 | O(12)–Cd–O(12A) | 75 |
| O(2)–Cd–O(12) | 98 | O(12)–Cd–O(22) | 53 |
| O(2)–Cd–O(12A) | 86 | O(12′)–Cd–O(22) | 128 |
| O(2)–Cd–O(22) | 98 | | |
| Tensor Element–Ligand Angles, deg | | | |
| $\sigma_{11}$–Cd–O(1) | 21 | $\sigma_{11}$–Cd–O(21) | 69 |
| $\sigma_{11}$–Cd–O(2) | 163 | $\sigma_{11}$–Cd–O(22) | 92 |
| $\sigma_{11}$–Cd–O(11) | 72 | $\sigma_{11}$–Cd–O(12A) | 99 |
| $\sigma_{11}$–Cd–O(12) | 98 | | |
| $\sigma_{22}$–Cd–O(1) | 74 | $\sigma_{22}$–Cd–O(21) | 159 |
| $\sigma_{22}$–Cd–O(2) | 107 | $\sigma_{22}$–Cd–O(22) | 42 |
| $\sigma_{22}$–Cd–O(11) | 121 | $\sigma_{22}$–Cd–O(12A) | 87 |
| $\sigma_{22}$–Cd–O(12) | 14 | | |
| $\sigma_{33}$–Cd–O(1) | 103 | $\sigma_{33}$–Cd–O(21) | 91 |
| $\sigma_{33}$–Cd–O(2) | 87 | $\sigma_{33}$–Cd–O(22) | 48 |
| $\sigma_{33}$–Cd–O(11) | 37 | $\sigma_{33}$–Cd–O(12A) | 172 |
| $\sigma_{33}$–Cd–O(12) | 101 | | |

(10) Charles, N. G.; Griffith, E. A. H.; Rodesiler, P. F.; Amma, E. L. *Inorg. Chem.* **1983**, *22*, 2717.

(11) Li, H.; Amma, E. L. *Inorg. Chem.*, to be submitted for publication.

(12) Inners, R. R.; Doty, F. D.; Garber, A. R.; Ellis, P. D. *J. Magn. Reson.* **1981**, *45*, 503.

(13) Pines, A.; Gibby, M. E.; Waugh, J. S. *J. Chem. Phys.* **1973**, *59*, 569.

(14) Rollett, J. S. *Computing Methods in Crystallography*; Pergamon Press: New York, 1975, p 22.

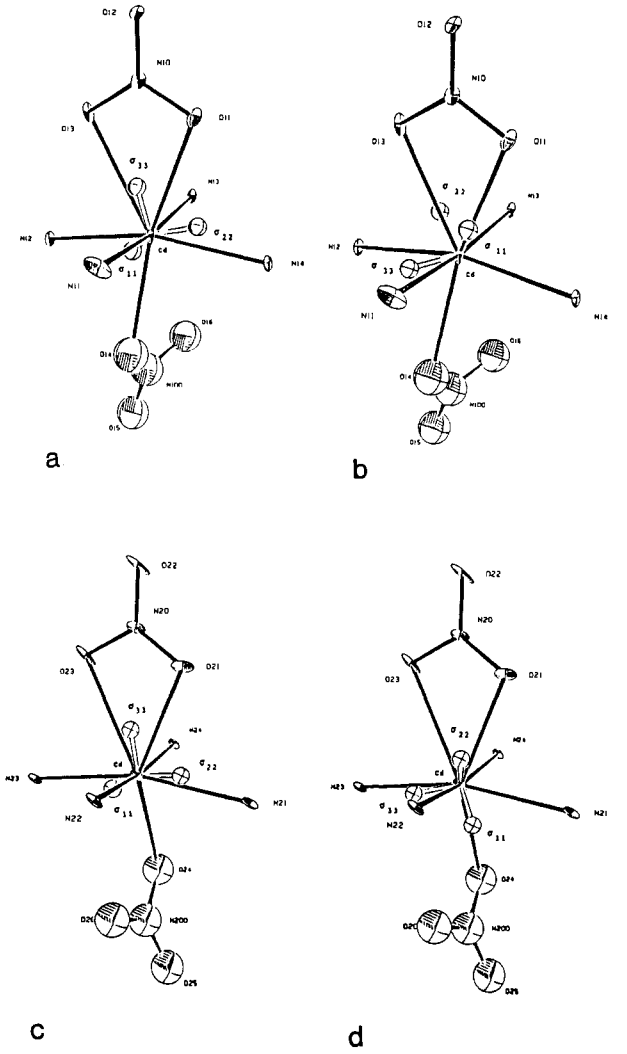


**Figure 7.** Ortep diagrams, showing the alternative orientations of the experimentally determined shielding tensors at the *xyz* and *x'y'z'* lattice sites for Cd–picoline. Parts a and c demonstrate, preferred orientations, whereas parts b and d demonstrate nonpreferred orientations. The nitrate molecule atoms represented by isotropic spheres (N(100), O(14), O(15), O(16) and N(200), O(24), O(25), O(26)) indicate disordered nitrate groups.

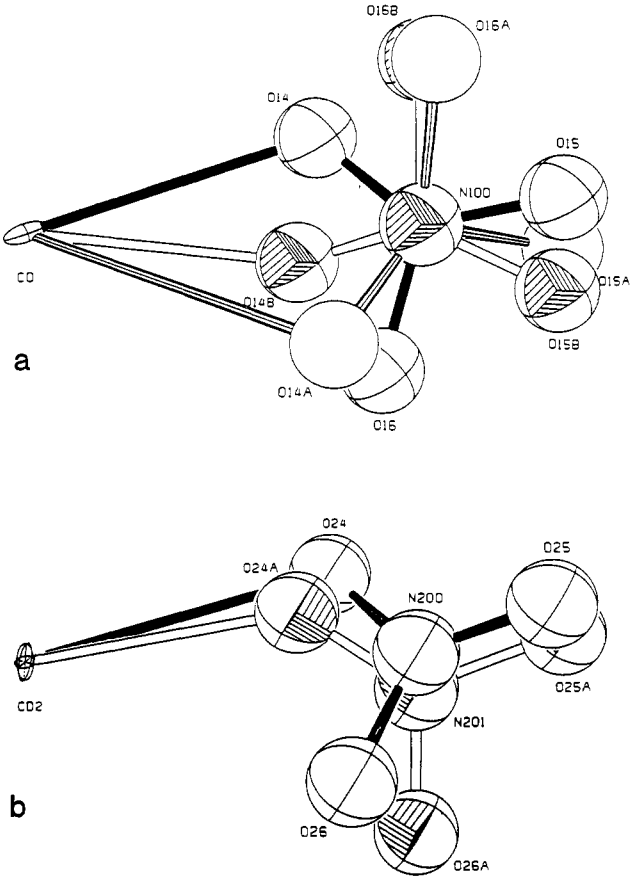


**Figure 8.** Ortep diagrams, showing the preferred orientations of the disordered nitrate group at the (a) *xyz* and (b) *x'y'z'* lattice sites for Cd–picoline.

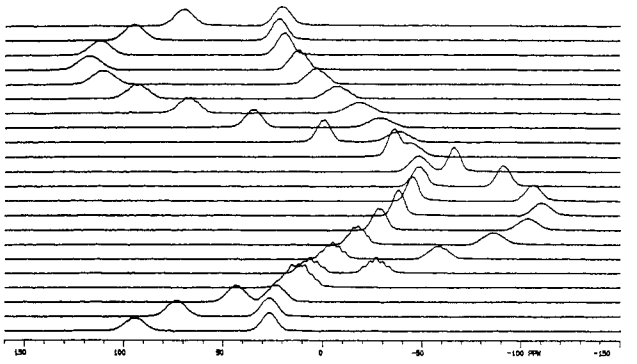

**Figure 9.** Rotation plot for Cd–picoline about the $a^*$ axis. The bottom spectrum is at 0° rotation angle. The top spectrum is at 191.1° rotation angle. The intervening spectra are at 9.1° intervals. Data acquisition parameters are described in the text.

Given this geometry, the transformation or projection matrix is derived to be

$$L = \begin{bmatrix} a \sin\beta \sin\gamma^* & 0 & 0 \\ -a \sin\beta \cos\gamma^* & b \sin\alpha & 0 \\ a \cos\beta & b \cos\alpha & c \end{bmatrix}$$

where $\alpha$, $\beta$, and $\gamma$ are the interaxial angles of the natural unit cell, $\cos\gamma^* = (\cos\alpha \cos\beta - \cos\gamma)/(\sin\alpha \sin\beta)$, and $\sin\gamma^* = (1 - \cos^2\gamma^*)^{1/2}$. The oblique basis is then projected into the orthogonal basis by

$$X' = LX$$

where $X$ is a vector in the natural basis and $X'$ is a vector in the orthogonalized basis. To orient monoclinic crystals via crystallographic camera techniques, we have previously aligned the symmetry axis, or *b* axis, via the Weissenberg oscillation method[15] and then aligned the *c* axis via the Laue technique.[15] This is consistent with Rollett's orthogonalization method.

For the triclinic tetrakis(4-picoline)(nitrato-*O*,*O'*)(nitrato-*O*)cadmium(II) single crystal, the following method was used to orient the orthogonalized unit cell with respect to the orthogonal cube reference frame. The natural *c* axis was aligned via the Weissenberg technique. The resulting rotation axis was referenced to the *x* axis in Rollett's geometry. This provided the $\alpha$ and $\beta$ angles of the nontrue Euler transformation matrix (i.e. the rotations are about fixed goniometer axes). With the natural *c* axis aligned with the *z* axis in Rollett's geometry, the *b* axis is then rotated into the *y*–*z* plane of the orthogonal frame (see Figure 1). One must keep in mind that the right-handed orthogonal frame as defined by Rollett is constrained to be coincident with the fixed orthogonal cube frame. Therefore, once the *z* axis is assigned to a cube axis, the remaining cube axes are automatically assigned according to a right-handed convention. In order to rotate the *b* axis into the *y*–*z* plane of the cube, the *b* axis is also found by the Weissenberg method. Given the angles required to align the *b* axis, the coordinates for the tip of the *b* basis vector before alignment are determined. This is accomplished by first translating the origin of a unit cell (with the *b* axis aligned) to the origin of the cube frame (at this point the coordinates for the *b* vector are $b(0,b,0)$). Then, application of the reverse rotation to the $b(0,b,0)$ vector, using the angles determined to align the *b* axis, yields a vector with coordinates $b = b(x,y,z)$ that determine the orientation of the basis vector before alignment. The *b* vector

(15) Buerger, M. J. *X-ray Crystallography*; Wiley: New York, 1942.

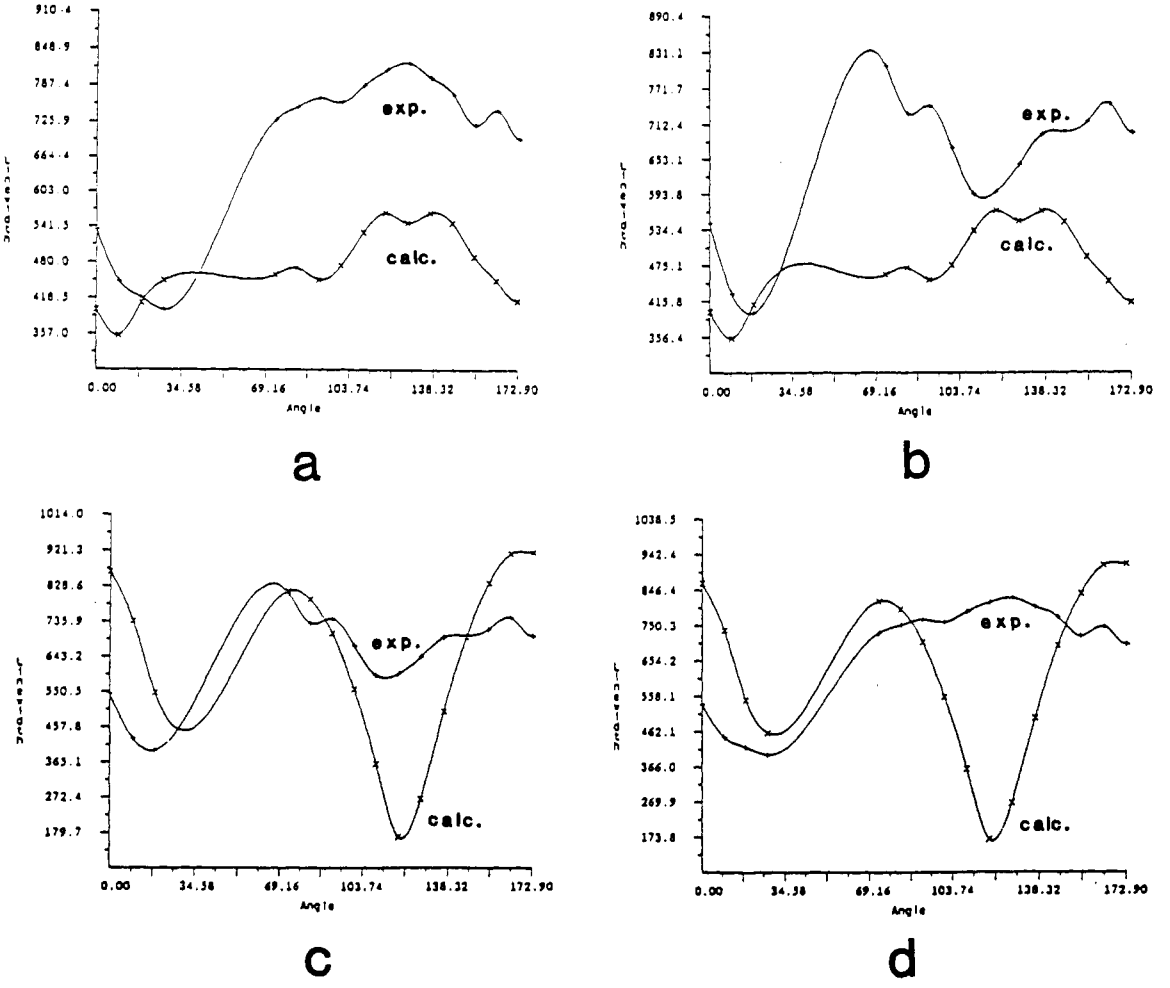


**Figure 10.** Line width plotted as a function of rotation angle about the $a^*$ axis for Cd–picoline. Part a shows the experimental line width (+) for tensor **A**, Table III, and the calculated line width (×) for the *xyz* lattice site. Part b shows the experimental line width (+) for tensor **B**, Table III, and the calculated line width (+) for the *xyz* lattice site. Part c shows the experimental line width (+) for tensor **B**, Table III, and the calculated line width (×) for the $x'y'z'$ lattice site. Part d shows the experimental line width (+) for tensor **A**, Table III, and the calculated line width (×) for the $x'y'z'$ lattice site.

along with the cube is then rotated such that the cube is coincident with the starting orientation for the alignment of the *c* axis (where the coordinates of the *b* vector remain $b(x,y,z)$). The *b* vector is then rotated according to the $\alpha$ and $\beta$ angles necessary to align the *c* axis, generating the coordinates for the *b* vector when the *c* axis is aligned with the *z* axis in Rollett's geometry ($b = b(x',y',z')$). In order to find the angle through which the *b* vector must be rotated about the *z*,*c* axis to bring the *b* axis into the *y*–*z* plane, the *b* vector is first projected into the *x*–*y* plane ($b^{x-y} = b(x',y',0)$) and then the scalar product of $b^{x-y}$ with the projection of $b^{x-y}$ into the *y*–*z* plane ($b^{x-y/y-z} = b(0,y',0)$ (shown in Figure 2) is calculated to find $\gamma$, i.e. the third nontrue Euler angle needed for the complete alignment of the triclinic crystal.

## Results and Discussion

**$[(C_6H_4OHCOO)_2Cd{\cdot}2H_2O]_2$.** Bis($\mu$-*o*-hydroxybenzoato)bis(*o*-hydroxybenzoato)tetraaquodicadmium(II), i.e. Cd–salicylate, crystallizes in the monoclinic space $P2_1/a$. Charles et al.[10] solved the crystal structure with the cadmium in the general position. The point group symmetry is expected to generate two distinguishable tensors. Experimentally, two resonances were observed for rotations about the $a^*$ and $c^*$ axes ($a^*$ and $c^*$ are the orthogonalized unit cell axes); however, the angular dependence of the chemical shift was quite similar for each lattice site. The rotation about the $a^*$ axis, which is shown in Figure 3, demonstrates the angular dependence described above. A single resonance was observed for rotation about the $b^*$ axis, i.e. the crystallographic 2-fold axis. The $^{113}$Cd chemical shielding tensor and the corresponding direction cosines for both the *xyz* and $\bar{x}y\bar{z}$ positions are given in Table I. From Table I, it can be shown that the experimentally determined eigenvectors are related by a 2-fold rotation about the *b* axis, i.e. $EV_{\bar{x}y\bar{z}} = R_{2b} \times EV_{xyz}$.

Cadmium salicylate crystallizes in the form of a dimer represented in Figure 4. The center of the dimer defines a crystallographic center of symmetry; therefore, these two cadmium nuclei are indistinguishable by an NMR experiment. For the following discussion, only half of this dimer will be represented when tensor orientations are shown. The $Cd^{2+}$ ion in crystals of Cd–salicylate is seven-coordinate. The ligand coordination geometry, shown in Figure 4, includes two pairs of bidentate benzoate carboxylate oxygen atoms, O(11), O(21) and O(12), O(22), where O(12) is a bridging atom, and a monodentate bridging benzoate carboxylate oxygen, O(12A), all contained in a plane with a greatest deviation of 0.15 Å, in addition to two axially coordinated water oxygen atoms. Each of the experimentally determined tensors is projected onto the molecular frame of the *xyz* site in Figure 5. As can be seen from Figure 5, the two tensors are nearly identically oriented. Given this result, it is expected that the two tensors should be nearly indistinguishable by the NMR experiment. This behavior was observed and is demonstrated by the quite similar angular dependence of the chemical shift for each lattice site shown in Figure 3. Figure 6 shows the *xyz* lattice site and its 2-fold-related lattice site translated to a common origin. From Figure 6, it is evident that the two lattice sites are nearly related by an identity symmetry operation, which is consistent with observations of similar tensor orientations and angular dependence of chemical shifts. Therefore, the assignment of which tensor belongs to the *xyz* lattice site is not possible and, due to the nearly congruent

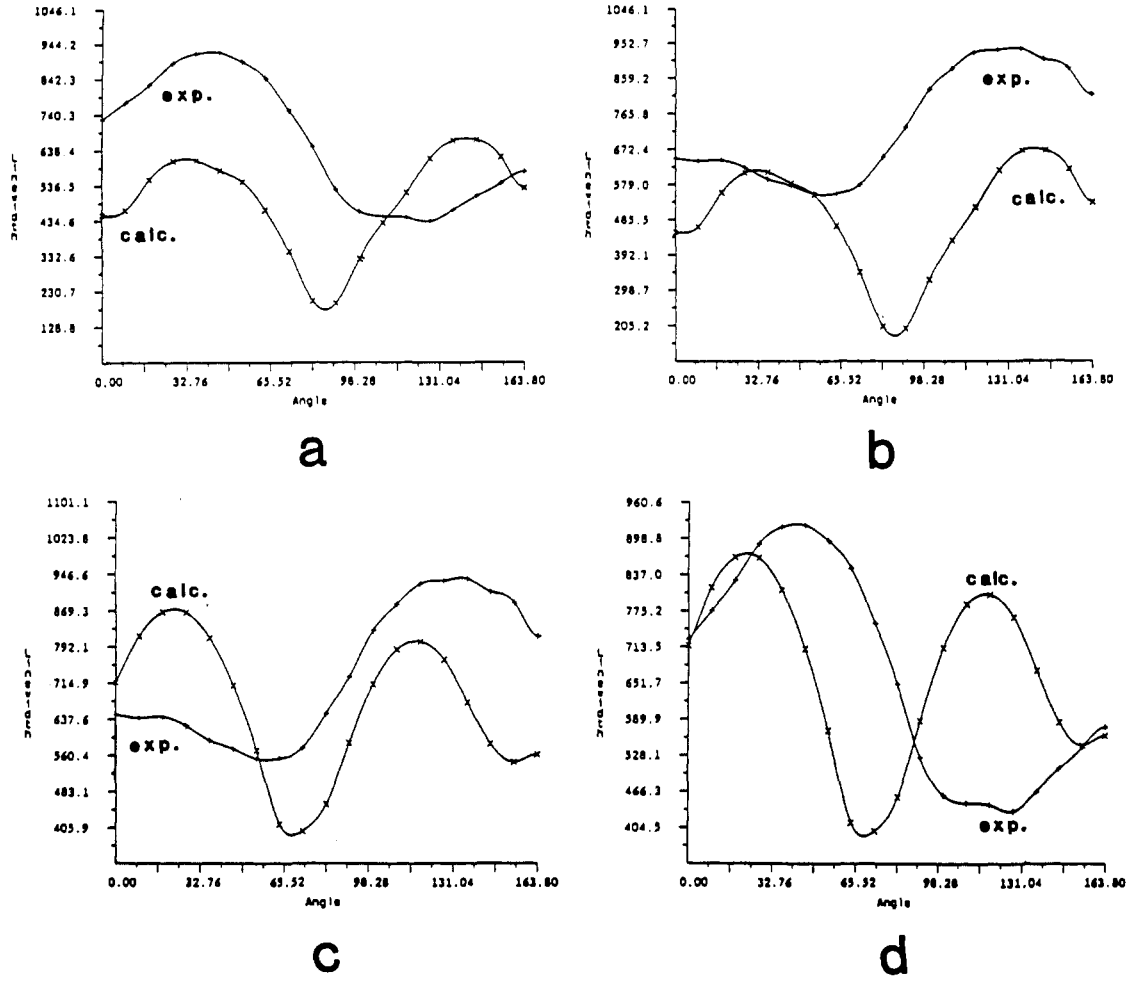


**Figure 11.** Line width plotted as a function of rotation angle about the $b^*$ axis for Cd–picoline. Part a shows the experimental line width (+) for tensor **A**, Table III, and the calculated line width (×) for the *xyz* lattice site. Part b shows the experimental line width (+) for tensor **B**, Table III, and the calculated line width (×) for the *xyz* lattice site. Part c shows the experimental line width (+) for tensor **B**, Table III, and the calculated line width (×) for the *x'y'z'* lattice site. Part d shows the experimental line width (+) for tensor **A**, Table III, and the calculated line width (×) for the *x'y'z'* lattice site.

tensor orientations, is not necessary to interpret the shielding contributions of the coordinating ligands.

The crystal structure has been described as isolated asymmetrically bridged dimers of diaquobis(*o*-hydroxybenzoato)cadmium(II).[10] The cadmium coordination sphere, which may be described as a pentagonal bipyramid, is illustrated in Figure 4 and detailed in Table II. The pentagonal plane is defined by one normal pair of bidentate carboxylate oxygens (O(12) and O(21)), one pair of bidentate carboxylate oxygens (in which one oxygen is two-coordinate (O(22)) and one oxygen is bridging and three-coordinate (O(12))), and a monodentate carboxylate oxygen, which is also bridging and three-coordinate (O(12′)). These five oxygen atoms form a BLS plane with a maximum deviation of 0.12 Å with the Cd 0.18 Å displaced toward O(2). The bridging oxygens (O(12) and O(12′)) are asymmetric in that O(12) contributes one long bond, i.e. 2.535 Å, to Cd and one short bond to the inversion-related Cd′, i.e. 2.271 Å. The remaining coordination is composed of two axial water oxygens in which the lone pair of electrons are directed in each case toward the cadmium atom. If the *xyz* site and tensor **A** from Table I are used, the most shielded element is found oriented at an angle of ~85° with respect to the pentagonal plane of carboxylate oxygens. This is consistent with the observations of Honkonen and Ellis,[1] where the shielding contribution due to carboxylate oxygens was found to be large and shielding. In the same investigation, it was determined that the shielding contribution due to water oxygens was large and deshielding. In accordance with this, the most deshielded tensor is experimentally found oriented at ~90° to the BLS line formed by O1 and O2.

**$[(C_6H_7N)_4Cd(NO_3)_2]$.** The crystal structure of the Cd–picoline complex has been solved by Li et al.[11] The complex crystallizes in the triclinic space $P\bar{1}$. The cadmium ion, which is seven-coordinate (see Figure 7), is ligated to four picoline molecules coordinated through the nitrogen atom in a poorly defined square plane. The nitrogen atom positions deviate from the BLS plane by as much as 0.25 Å. Furthermore, roughly axial to this plane, two oxygen atoms are coordinated through an ordered bidentate nitrate group, and an oxygen is coordinated through a disordered monodentate nitrate group. The lattice contains two crystallographically distinct cadmium sites. The existence of two distinct sites correlates with the disordered nitrate group having different preferred orientations at each lattice site, which is depicted in Figure 8. The disordered nitrate group is in part responsible for reducing the point group symmetry to $P\bar{1}$.

Two NMR-indistinguishable general positions are generated by the inversion symmetry operator for each crystallographically distinct lattice site, yielding four cadmium atoms per unit cell. A single resonance is expected for each of the two magnetically distinct sites and was observed for rotations about each of the cube axes. Figure 9 shows the angular dependence of the chemical shift for rotation about the natural crystallographic *c* axis. It can be seen from Figure 9 that each resonance has a different angular dependent natural line width. It is also evident in Figure 9 that, at particular rotation angles, the resonance yields structure in the line shape originating from the dipolar couplings. The difference of the angular dependence of the natural line width between the two crystallographically distinct lattice sites enables one to assign experimentally determined tensors to respective lattice sites.

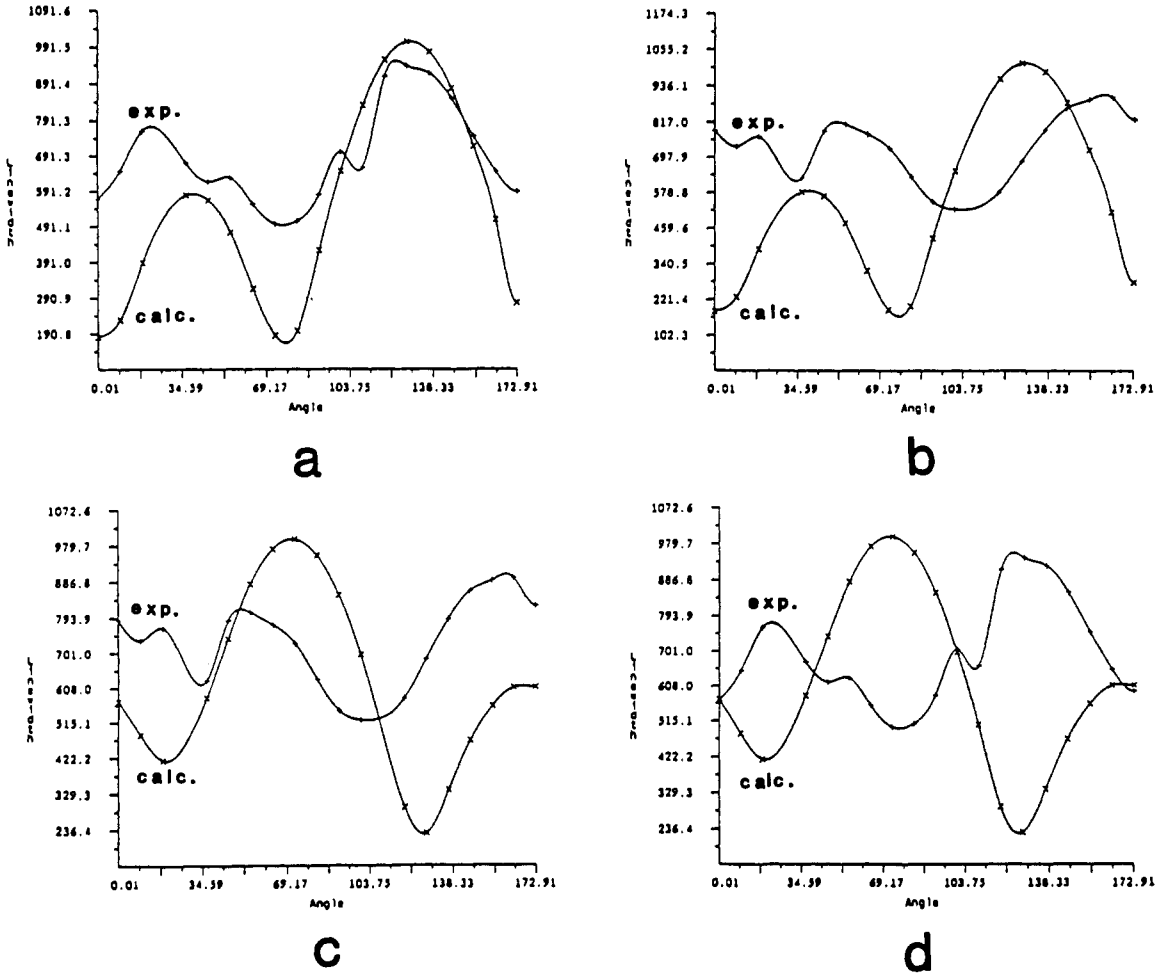


**Figure 12.** Line width plotted as a function of rotation angle about the *c* axis for Cd-picoline. Part a shows the experimental line width (+) for tensor **A**, Table III, and the calculated line width (×) for the *xyz* lattice site. Part b shows the experimental line width (+) for tensor **B**, Table III, and the calculated line width (×) for the *xyz* lattice site. Part c shows the experimental line width (+) for tensor **B**, Table III, and the calculated line width (×) for the *x'y'z'* lattice site. Part d shows the experimental line width (+) for tensor **A**, Table III, and the calculated line width (×) for the *x'y'z'* lattice site.

The problem of assigning symmetry-related tensors to lattice sites has been addressed by Honkonen and Ellis in part 3[16] of this series and by Marchetti et al. in part 4[17] of this series. In the above described experiments, the angular dependence arises due to dipolar coupling between the spin $I = {}^1/_2$ $^{113}$Cd nuclide and either the spin $I = {}^1/_2$ $^{13}$C nuclide[17] or the spin $I = 1$ $^{14}$N nuclide.[16] In general, the dipolar interaction Hamiltonian has the form[18]

$$H_D = \omega_D(A + B + C + D + E + F)$$

where $\omega_D = \gamma_{Cd}\gamma_N{}^h/2\pi r^3$ and $A + B + C + D + E + F$ is the standard "dipolar alphabet". To calculate the dipolar interaction, we make two important simplifying assumptions.

First, we assume that the interaction is simply additive and pairwise. Given this assumption, we can calculate a Zeeman plus dipolar spectrum from which the line width is approximated by the frequency difference between the $-I/2$ and $I/2$ transitions.[16] In this situation, $I$ refers to the $I_{max}$ for the vector addition of $n$ spins that are pairwise coupled; e.g., for a calculation involving $n = 32$ nitrogen atoms, $I_{max} = 32$. Only the $A$ and $B$ terms contribute to the dipolar splitting due to the content of spin operators and the selection rules.[18b] The effect of the dipolar interaction on the eigenvalues can then be calculated by evaluation of the matrix elements, $\langle i|H_D|j\rangle$, where $\langle i|$ $|j\rangle$ are spin eigenstates of the Zeeman Hamiltonian, $H_Z$. For the spin $I = {}^1/_2$ nucleus coupled to a spin $I = 1$ nucleus, the following spin product states can be defined:

$$|Q_{3/2}\rangle = |{}^1/_2,1\rangle$$

$$|Q_{1/2}\rangle = (1/\sqrt{2})(|{}^1/_2,0\rangle + |{}^{-1}/_2,1\rangle)$$

$$|Q_{-1/2}\rangle = (1/\sqrt{2})(|{}^{-1}/_2,0\rangle + |{}^1/_2,-1\rangle)$$

$$|Q_{-3/2}\rangle = |{}^{-1}/_2,-1\rangle$$

$$|D_{1/2}\rangle = (1/\sqrt{2})(|{}^1/_2,0\rangle - |{}^{-1}/_2,1\rangle)$$

$$|D_{-1/2}\rangle = (1/\sqrt{2})(|{}^{-1}/_2,0\rangle - |{}^1/_2,-1\rangle)$$

where Q and D refer to quartet and doublet states, respectively. Transitions are only allowed between quartet states or between doublet states, given the selection rules $\Delta m = \pm 1$ and $\Delta I = 0$.[18] For a spin $I = {}^1/_2$ cadmium nucleus coupled to a single spin $I = 1$ nitrogen nucleus, a three-line spectrum is calculated where two resonances occur at $\omega_0 \pm (1 - 3\cos^2\theta)\omega_D$ centered about a resonance at $\omega_0$. The approximated line width is given $[(\omega_0 + (1 - 3\cos^2\theta)\omega_D) - (\omega_0 - (1 - 3\cos^2\theta)\omega_D)]/2$. The angle, $\theta$, that

(16) Honkonen, R. S.; Marchetti, P. S.; Ellis, P. D. *J. Am. Chem. Soc.* **1986**, *108*, 912.
(17) Marchetti, P. S.; Honkonen, R. S.; Ellis, P. D. *J. Magn. Reson.* **1987**, *71*, 294.
(18) (a) Abragam, A. *Principles of Nuclear Magnetism*; Clarendon Press: Oxford, England, 1961; p 97. (b) Harris, R. K. *Nuclear Magnetic Resonance Spectroscopy*; Pitman Publishing: Marshfield, MA, 1983. p 95.

**Table III.** Direction Cosines Relating the Principal Elements of the $^{113}Cd$ Shielding Tensor to the Molecular Reference Frame in Cd–Picoline[a]

| tensor element[b] | chem shift, ppm[c] | direction cosines | | | angles, deg | | |
|---|---|---|---|---|---|---|---|
| | | $a^*$ | $b^*$ | $c^*$ | $a^*$ | $b^*$ | $c^*$ |
| | | A. *xyz* Cd Lattice Site | | | | | |
| $\sigma_{11}$ | −115 | 0.5278 | 0.6592 | 0.5353 | 58 | 49 | 58 |
| $\sigma_{22}$ | −37 | 0.8474 | −0.4508 | −0.2803 | 32 | 117 | 106 |
| $\sigma_{33}$ | 194 | −0.0565 | −0.6017 | 0.7967 | 93 | 126 | 37 |
| $\bar{\sigma}$ | 14 | | | | | | |
| | | B. *x'y'z'* Cd Lattice Site | | | | | |
| $\sigma_{11}$ | −115 | −0.7936 | −0.4524 | 0.4066 | 142 | 116 | 66 |
| $\sigma_{22}$ | −46 | 0.5804 | −0.3632 | 0.7287 | 54 | 111 | 43 |
| $\sigma_{33}$ | 184 | 0.1819 | −0.8144 | −0.5509 | 79 | 144 | 123 |
| $\bar{\sigma}$ | 8 | | | | | | |

[a] Eigenvectors and corresponding angles are with respect to the orthogonalized unit cell, $a^*$, $b^*$, $c^*$. [b] See footnote *b* of Table I. [c] The $^{113}Cd$ chemical shifts are reported with positive values to higher frequency/lower shielding relative to solid $Cd(ClO_4)_2 \cdot 6H_2O$.

each Cd–N bond makes with respect to the magnetic field and the Cd–N distance is needed to calculate the dipolar interaction for each lattice site at each rotation angle about the three cube axes. For our calculations, all the nitrogen atoms in a single unit cell were used. Beyond a single unit cell, the rotation-angle-dependent line width will simply be scaled for each lattice site.

Second, in this approximation, the possible second-order nature of the quadrupolar nuclei is ignored; i.e., the PAS frame of the dipolar interaction is assumed to be coincident with the PAS frame of the electric field gradient (EFG) tensor of each of the quadrupolar nitrogen nuclei.[19] This last assumption is not very likely but is intractable by simulation due to five parameters, i.e. quadrupole coupling constant, asymmetry, and EFG tensor elements, $V_{xx}$, $V_{yy}$, and $V_{zz}$, which are, in general, different for each nitrogen nucleus in the coordination sphere of the cadmium nucleus. Therefore, admittedly, our calculation is not exact yet appears to be informative even with these assumptions.

Figures 10–12 show the calculated and experimental line widths for both the *xyz* and *x'y'z'* lattice sites for rotations roughly about the $a^*$, $b^*$, and $c^*$ axes (a*, b*, and c* designate the orthogonalized unit cell basis), respectively. It is immediately obvious that, *quantitatively*, the calculated function fits the experimental line width rather poorly, which is not surprising given the assumptions discussed above. However, qualitative features, such as line width minima and maxima as a function of angle, appear to be in sufficient agreement with calculated features to allow assignment of the observed resonance to its respective lattice site.

Figure 10a shows line-width data for the resonance corresponding to tensor **A** in Table III (+) and the calculated line width for the *xyz* lattice site (×) for a rotation about the $a^*$ axis. In Figure 10a, both experimental and calculated line widths reach a maximum at about 130°. In contrast, Figure 10b shows that the experimental line width corresponding to the resonance of tensor **B** in Table III has a minimum at 130°, corresponding to a line width maximum calculated for the *xyz* lattice site. However, Figure 10c shows that the line width of the resonance for tensor **B** in Table III qualitatively matches four features of the *x'y'z'* lattice site, namely, line-width minima at about 30 and 120° and line-width maxima at 65 and 170°. Whereas, in Figure 10d, the line width of the resonance for tensor **A** exhibits a maximum at 120°, where the *x'y'z'* lattice site reaches a minimum at 120°. The line-width difference at 120° is about 700 Hz. Therefore, from this data, tensor **A** in Table III can be assigned to the *xyz* lattice site.

Figure 11 shows the line-width data for rotations about the *b'* axis. Figure 11a,c shows the preferred tensor lattice site pairings. Figure 11a,c does not exhibit significantly different features to allow assignment. However, Figure 11c demonstrates three coincident features, i.e. line-width maxima at 20 and 130° and line-width mimina at 65°. Again, Figure 10d shows significant disagreement between the line width for resonance of tensor **A** of Table III with the *x'y'z'* lattice site. Specifically, a line-width maximum occurs at 130° for the *x'y'z'* lattice site, where, correspondingly, a line-width minimum occurs at 130° for the resonance of tensor **A** in Table III. Again, the line width of the resonance for tensor **A** in Table III behaves most similar to that of the *xyz* lattice site.

Finally, Figure 12 shows the line-width data for rotation about the natural *c* axis of the unit cell. Figure 12a demonstrates a rather good fit of the line width of tensor **A** in Table III to that of the *xyz* lattice site. Line-width maxima occur at 40 and 135° in both resonances, and a line-width minimum occurs at 70° in both. Clearly, the match is less favorable in Figure 12b. In Figure 12c, line-width minima occur roughly at 20 and 120° with a maximum at about 70° for both tensor **B** in Table III and the *x'y'z'* site. However, in Figure 12d, each line-width minimum in the *x'y'z'* lattice site corresponds to a line-width maximum in the resonance for tensor **A** in Table III.

In summary, for each rotation axis, the line-width data support the assignment of tensor **A** and tensor **B** in Table III to the *xyz* and *x'y'z'* lattice sites, respectively.

Figure 7 shows the two experimentally determined tensors projected onto the molecular frame of the *xyz* and *x'y'z'* sites. On the basis of empirical observations that nitrogen ligands are deshielding compared to oxygen atoms[9] and the orthogonal interaction of the chemical shielding tensor,[20-22] the orientations depicted in Figure 7a for the *xyz* lattice site and correspondingly in Figure 7b for the *x'y'z'* lattice site are preferred. In each case the most deshielded tensor element, $\sigma_{33}$, is nearly perpendicular to the plane defined by the coordination of the four picoline molecules. Specifically, $\sigma_{33}$ makes an angle of 75° with the BLS

**Table IV.** Structural Data for Cadmium Picoline: Interatomic Distances and Angles for the Primary Coordination Sphere and Details of Tensor Ligand Geometry for the *xyz* Cd Lattice Site

| | | | |
|---|---|---|---|
| Interatomic Distances, Å | | | |
| Cd(1)O(11) | 2.55 | Cd(1)–N(12) | 2.36 |
| Cd(1)–O(13) | 2.69 | Cd(1)–N(13) | 2.35 |
| Cd(1)–O(14) | 2.50 | Cd(1)–N(14) | 2.37 |
| Cd(1)–N(11) | 2.35 | | |
| Interatomic Angles, deg | | | |
| O(11)–Cd(1)–O(13) | 48 | O(14)–Cd(1)–N(11) | 76 |
| O(11)–Cd(1)–O(14) | 155 | O(14)–Cd(1)–N(12) | 78 |
| O(11)–Cd(1)–N(11) | 86 | O(14)–Cd(1)–N(13) | 112 |
| O(11)–Cd(1)–N(12) | 120 | O(14)–Cd(1)–N(14) | 86 |
| O(11)–Cd(1)–N(13) | 86 | N(11)–Cd(1)–N(12) | 92 |
| O(11)–Cd(1)–N(14) | 77 | N(11)–Cd(1)–N(13) | 172 |
| O(13)–Cd(1)–O(14) | 144 | N(11)–Cd(1)–N(14) | 91 |
| O(13)–Cd(1)–N(11) | 84 | N(12)–Cd(1)–N(13) | 91 |
| O(13)–Cd(1)–N(12) | 72 | N(12)–Cd(1)–N(14) | 163 |
| O(13)–Cd(1)–N(13) | 89 | N(13)–Cd(1)–N(14) | 89 |
| O(13)–Cd(1)–N(14) | 125 | | |
| Tensor Element–Ligand Angles, deg | | | |
| $\sigma_{11}$–Cd(1)–O(11) | 88 | $\sigma_{11}$–Cd(1)–N(12) | 94 |
| $\sigma_{11}$–Cd(1)–O(13) | 89 | $\sigma_{11}$–Cd(1)–N(13) | 174 |
| $\sigma_{11}$–Cd(1)–O(14) | 73 | $\sigma_{11}$–Cd(1)–N(14) | 88 |
| $\sigma_{11}$–Cd(1)–N(11) | 4 | | |
| $\sigma_{22}$–Cd(1)–O(11) | 54 | $\sigma_{22}$–Cd(1)–N(12) | 173 |
| $\sigma_{22}$–Cd(1)–O(13) | 102 | $\sigma_{22}$–Cd(1)–N(13) | 85 |
| $\sigma_{22}$–Cd(1)–O(14) | 109 | $\sigma_{22}$–Cd(1)–N(14) | 23 |
| $\sigma_{22}$–Cd(1)–N(11) | 91 | | |
| $\sigma_{33}$–Cd(1)–O(11) | 144 | $\sigma_{33}$–Cd(1)–N(12) | 96 |
| $\sigma_{33}$–Cd(1)–O(13) | 168 | $\sigma_{33}$–Cd(1)–N(13) | 93 |
| $\sigma_{33}$–Cd(1)–O(14) | 26 | $\sigma_{33}$–Cd(1)–N(14) | 67 |
| $\sigma_{33}$–Cd(1)–N(11) | 94 | | |

(19) Hexem, J. G.; Frey, M. H.; Opella, S. J. *J. Chem. Phys.* **1982**, *77*, 3847.
(20) Mehring, M. *Principles of High Resolution NMR in Solids*; Springer-Verlag: Berlin, 1983.
(21) Jakobsen, H. J.; Ellis, P. D.; Inners, R. R.; Jensen, C. F. *J. Am. Chem. Soc.* **1982**, *104*, 7442.
(22) Kennedy, M. A.; Ellis, P. D. *J. Am. Chem. Soc.*, in press.

**Table V.** Structural Data for Cadmium Picoline: Interatomic Distances and Angles for the Primary Coordination Sphere and Details of Tensor Ligand Geometry for the $x'y'z'$ Cd Lattice Site

| | | | |
|---|---|---|---|
| Interatomic Distances, Å | | | |
| Cd(2)-O(21) | 2.52 | Cd(2)-N(22) | 2.33 |
| Cd(2)-O(23) | 2.72 | Cd(2)-N(23) | 2.38 |
| Cd(2)-O(24) | 2.64 | Cd(2)-N(24) | 2.35 |
| Cd(2)-N(21) | 2.39 | | |
| Interatomic Angles, deg | | | |
| O(21)-Cd(2)-O(23) | 47 | O(24)-Cd(2)-N(21) | 79 |
| O(21)-Cd(2)-O(24) | 148 | O(24)-Cd(2)-N(22) | 113 |
| O(21)-Cd(2)-N(21) | 76 | O(24)-Cd(2)-N(23) | 87 |
| O(21)-Cd(2)-N(22) | 86 | O(24)-Cd(2)-N(24) | 74 |
| O(21)-Cd(2)-N(23) | 119 | N(21)-Cd(2)-N(22) | 89 |
| O(21)-Cd(2)—N(24) | 86 | N(21)-Cd(2)-N(23) | 165 |
| O(23)-Cd(2)-O(24) | 149 | N(21)-Cd(2)-N(24) | 91 |
| O(23)-Cd(2)-N(21) | 123 | N(22)-Cd(2)-N(23) | 90 |
| O(23)-Cd(2)-N(22) | 90 | N(22)-Cd(2)-N(24) | 172 |
| O(23)-Cd(2)-N(23) | 72 | N(23)-Cd(2)-N(24) | 93 |
| O(23)-Cd(2)-N(24) | 84 | | |
| Tensor Element-Ligand Angles, deg | | | |
| $\sigma_{11}$-Cd(2)-O(21) | 85 | $\sigma_{11}$-Cd(2)-N(22) | 169 |
| $\sigma_{11}$-Cd(2)-O(23) | 89 | $\sigma_{11}$-Cd(2)-N(23) | 100 |
| $\sigma_{11}$-Cd(2)-O(24) | 72 | $\sigma_{11}$-Cd(2)-N(24) | 8 |
| $\sigma_{11}$-Cd(2)-N(21) | 83 | | |
| $\sigma_{22}$-Cd(2)-O(21) | 60 | $\sigma_{22}$-Cd(2)-N(22) | 80 |
| $\sigma_{22}$-Cd(2)-O(23) | 107 | $\sigma_{22}$-Cd(2)-N(23) | 170 |
| $\sigma_{22}$-Cd(2)-O(24) | 97 | $\sigma_{22}$-Cd(2)-N(24) | 97 |
| $\sigma_{22}$-Cd(2)-N(21) | 18 | | |
| $\sigma_{33}$-Cd(2)-O(21) | 30 | $\sigma_{33}$-Cd(2)-N(22) | 86 |
| $\sigma_{33}$-Cd(2)-O(23) | 17 | $\sigma_{33}$-Cd(2)-N(23) | 89 |
| $\sigma_{33}$-Cd(2)-O(24) | 160 | $\sigma_{33}$-Cd(2)-N(24) | 87 |
| $\sigma_{33}$-Cd(2)-N(21) | 106 | | |

plane of Cd and the four nitrogen atoms at the $xyz$ site and an angle of 82° at the $x'y'z'$ site. Clearly, the orientation of the most deshielded element is determined by the shielding contribution of the coordinated nitrogen atoms. The data in Tables IV and V indicate that the orientation of the most shielded element is determined by the plane defined by the $Cd^{2+}$ ion and the bidentate nitrate ligand. At the $xyz$ lattice site, the $\sigma_{11}$ element is oriented at 83° with respect to the Cd-bidentate nitrate ligand plane, and at 81° at the $x'y'z'$ lattice site. Therefore, from the $xyz$ to $x'y'z'$ lattice site, two ligand features dominate the orientation of the shielding tensor; namely, the square plane defined by the Cd ion and the four picoline nitrogen atoms determines the orientation of the most deshielded tensor element, whereas the plane defined by the Cd ion and the two bidentate nitrate oxygen atoms determines the orientation of the most shielded tensor element.

## Conclusion

The orientation of the chemical shielding tensor in the dimer of diaquobis(2-hydroxybenzoato)cadmium(II) was found to be determined by the axial bonding interaction of water oxygen atoms in the case of the most deshielded tensor element and by a pentagonal plane of a monodentate benzoate carboxylate oxygen atom and two pairs of bidentate benzoate carboxylate oxygen atoms in the case of the most shielded tensor element. It was found that a special geometrical relationship between the $xyz$ site and its 2-fold-related site did not allow, nor made necessary, the assignment of each experimentally determined shielding tensor to its respective lattice site.

In tetrakis(4-picoline)(nitrato-*O*,*O*')(nitrato-*O*)cadmium(II), the two experimentally determined shielding tensors were found to have nearly identical orientations at each of the crystallographically distinct sites. At each site, the tensor orientation was determined by a common feature. Precisely, the orientation of the most deshielded tensor element was determined by the square plane of picoline nitrogen atoms. The orientation of the most shielded tensor element was determined by the plane defined by the $Cd^{2+}$ ion and the bidentate nitrate oxygen atoms at each lattice site. It was shown that a calculation of the expected line width for each lattice site as a function of the rotation angle with respect to the magnetic field was sufficient to confirm the assignment of the experimentally determined shielding tensors to crystallographically distinct lattice sites. The assignment based on empirical observations with respect to shielding contributions of different ligand identities and observed symmetries is consistent with the assignment based on the angular dependence of the line width for each lattice site.

Finally, it is evident that these observations support the previously established ideas concerning ligand identity with respect to shielding contributions and the growing realization of the importance of ligand geometry in determining the orientation of shielding tensors.

**Acknowledgment.** We are grateful to the National Institutes of Health, via Grant GM 26295, for partial support of this work. Further, we acknowledge the National Science Foundation, via Grant CHE86-13421, for the purchase of the DEC MicroVax II computer. Finally, we acknowledge Drs. Betty Griffith and Paul Marchetti for the preparation of the picoline and salicylate crystals, respectively.

**Registry No.** $[(C_6H_4OHCOO)_2Cd\cdot 2H_2O]_2$, 40937-33-5; $[(C_6H_7N)_4Cd(NO_3)_2]$, 124685-76-3; $^{113}$Cd, 14336-66-4.